Pergamon

Int. J. Heat Mass Transfer. Vol. 39, No. 14, pp. 3035–3043, 1996

0017–9310/96 $15.00 + 0.00

0017–9310(95)00331–2

Numerical simulation of heat transfer in floating zone single crystal growth process with radio-frequency induction heating

Y. MASUDA
Tohoku National Industrial Research Institute, 4-2-1, Nigatake, Miyagino-ku, Sendai, 983 Japan

T. TSUKADA and M. HOZAWA
Institute for Chemical Reaction Science, Tohoku University, 2-1-1, Katahira, Aoba-ku, Sendai, 980 Japan

N. IMAISHI
Institute of Advanced Material Study, Kyushu University, 6-1, Kasugakouen, Kasuga, 816 Japan

and

N. OHNISHI
Japan Space Utilization Promotion Center, 3-30-16, Nishiwaseda, Shinjuku-ku, Tokyo, 169 Japan

(*Received* 15 *June* 1995 *and in final form* 21 *August* 1995)

Abstract—Analysis of heat transfer in the floating zone (FZ) crystal growth system with a radio-frequency (RF) induction heating is carried out, using the hybrid finite element and boundary element method for calculation of the electromagnetic and temperature fields, and applying the coordinate transformation method to represent exactly the unknown shapes of phase boundaries in the system. The effects of processing parameters, such as the RF current frequency, on FZ growth is investigated numerically, and a diagram for the upper and lower limits of the current density in the RF coil between which the molten zone can be stable is proposed. Copyright © 1996 Elsevier Science Ltd.

1. INTRODUCTION

One of the methods of the production of high-purity single crystals is the floating zone (FZ) technique. In this technique, a relatively small zone of feed material in the form of a free-standing rod is melted by suitable heating equipment, and a single crystal is grown by moving the molten zone through the whole length. As the floating-zone melting can be processed without a crucible, the contamination of melt from the crucible can be avoided. For instance, the silicon crystal with the oxygen content two orders of magnitude lower by the FZ technique can be obtained in comparison with the Czochralski silicon. A radio-frequency (RF) induction heating is commonly used to achieve melting in the FZ process as shown in Fig. 1, especially for the semiconductor materials with high electric conductivity, although there are many other heating methods such as thermal or light radiative methods. High frequency electric current in the RF coil induces an eddy current in the conductor, feed rod, which is melted by Joulean heating from the current. The electromagnetic field caused by the RF current also plays an important role in determining the shape and stability of the molten zone and the hydrodynamics in the melt through the Lorentz force.

For the production of a perfect single crystal, it is important to acquire correct knowledge about the heat transfer and the melt convection, and to control them in the FZ equipment, because the crystal quality is closely related to the transport phenomena in the furnace. One of the methods used to understand the phenomena occurring during FZ crystal growth is numerical simulation. In particular, a mathematical model which can predict simultaneously the temperature field in the system, the melt hydrodynamics and the shapes of phase boundaries is useful. Extensive studies on such a mathematical model have recently been carried out, for an FZ growth system with thermal radiative heating. For instance, Duranceau *et al.* [1] carried out a numerical simulation for the silicon FZ crystal growth processes using a conduction-dominated thermal-capillary model, and investigated the effects of the processing parameters such as the crystal growth rate on the temperature distributions and interface shapes in the FZ system. Lan *et al.* [2–4] computed the melt convections as well as the temperature field and all interface shapes

NOMENCLATURE

A	angular magnetic vector potential
Bo	Bond number
Bo_e	electromagnetic Bond number
B_s	tangential magnetic field
c_p	heat capacity [J kg^{-1} K^{-1}]
f	meniscus shape function
G	response function
g	gravitational acceleration [m s^{-2}]
H	curvature of the meniscus
ΔH_f	heat of fusion [J kg^{-1}]
N_A	non-dimensional number defined by equation (2)
N_Q	non-dimensional number defined by equation (5)
J	current density
J_c'	dimensional forced current density in RF coil [A m^{-2}]
n	outward normal unit
Pe	Peclet number
Q	heat generation rate
q	normal derivatives of A
R_s	radius of crystal [m]
Ra	radiation number
r	radial distance in cylindrical coordinates
St	Stefan number
T	temperature
T_a	effective ambient temperature
T_{melt}^{*}	dimensional temperature of silicon melting point [K]
t	time
V	crystal growth rate [m s^{-1}]
z	axial distance in cylindrical coordinates.

Greek symbols

α	electrical conductivity ratio
α'	electrical conductivity [S m^{-1}]
ε	emissivity
γ	surface tension [N m^{-1}]
κ	thermal conductivity ratio
κ'	thermal conductivity [W m^{-1} K^{-1}]
λ	reference pressure difference
μ_0	magnetic permeability in free space [H m^{-1}]
ρ	density [kg m^{-3}]
φ_0	growth angle [rad]
ω	frequency [Hz].

Subscripts

a	free space
c	RF coil
f	feed
m	melt
s	single crystal.

during the FZ crystal growth of $NaNO_3$ and silicon under the normal- and micro-gravity, and demonstrated numerically the effect of Marangoni convection on the interface shapes. While there have been few theoretical studies in the FZ system with RF heating, because the electromagnetic field must be computed additionally and the electromagnetic force generated by the field affects complicatedly the growth system. Mühlbauer *et al.* [5] computed the magnetohydrodynamics convection in the silicon melt for the practical needle-eye FZ growth system, and revealed that the electromagnetic force exceeds all other forces by several orders of magnitude and the flow caused by the force is dominant in the melt. Riahi *et al.* [6] analyzed the effect of electromagnetic force on the shape of the melt surface in RF FZ system, and showed that the shape and stability of the molten zone depend upon the electromagnetic Bond number as well as the gravitational Bond number.

This study's main goal is to make a program for calculating a total floating zone furnace. As a first step, we ignore the effect of melt convection. The purpose of the present work is to develop a mathematical model, based on the conduction-dominated heat transfer in a small FZ crystal growth system with a RF heating, which can predict the temperature and electromagnetic fields as well as all interface shapes in the system, and to extract the processing factors which affect the silicon FZ crystal growth. Melt convection was not taken into account in the present model, because the Prandtl number of silicon melt is relatively small and thus it seems that the melt convection could not strongly affect the temperature field in the melt.

2. MATHEMATICAL MODEL

The FZ crystal growth system with a radio frequency heating, which consists of the feed rod, the melt, the single crystal and the one-turn RF coil as shown in Fig. 1, is considered here. As the electromagnetic field generated by the RF coil current plays an important role in the deformation of the melt surface as well as the Joulean heating, the analysis of the electromagnetic field must be coupled with that of the heat transfer in the system. In the present work, a conduction-dominated heat transfer model in which melt convection is neglected is used, although the electromagnetic force also induces the magnetohydrodynamic convection in the melt in addition to the natural and Marangoni convections in the RF FZ system.

Any quantitative analysis of electromagnetic

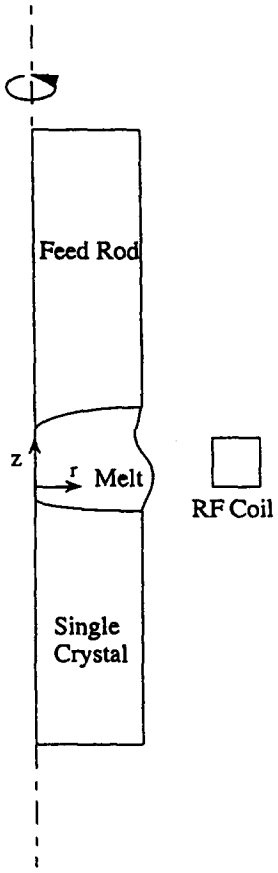

Fig. 1. FZ crystal growth system with a radio frequency heating.

phenomena must commence with Maxwell's equations. The following are assumed in the analysis: (1) the system is axially symmetric; (2) the media are linear, isotropic and stationary; (3) the displacement current is unimportant in this situation and (4) there is no net charge in the system. Under these assumptions, Maxwell's equation can be transformed into the following non-dimensional equation in cylindrical coordinates.

$$\frac{1}{r}\frac{\partial}{\partial r}\left(r\frac{\partial A_i}{\partial r}\right)+\frac{\partial^2 A_i}{\partial z^2}-\frac{A_i}{r^2}=-J_i \quad i=\text{s, m, f, c or a} \tag{1}$$

where the single crystal, the melt, the feed rod, the RF coil and free space are denoted by the subscripts 's', 'm', 'f', 'c' and 'a', respectively. J_i and A_i are the non-dimensional angular components of the current density and the vector potential, respectively, and are normalized with the single crystal radius and the forced current density in the RF coil. As every physical quantity can be assumed to have the conventional harmonic time dependency, $\exp(2\pi j\omega t)$, J_i in equation (1) is given by $-j\alpha_i N_A A_i$ in the conductor 'i', i.e. the feed rod, the melt, the single crystal and the RF coil, and by zero in free space. In addition, the forced current should be considered in the RF coil. N_A is a non-dimensional number defined by

$$N_A=\mu_0\omega\alpha_s' R_s^2 \tag{2}$$

where μ_0 is magnetic permeability in space and α_s' is the dimensional electric conductivity of a single crystal.

In the conduction-dominated model of heat transfer in the FZ system, we assume that the system is axisymmetric and quasi-steady. Under these assumptions, the non-dimensional energy equations are given as follows, where the single crystal radius and the melting-point temperature are used as the characteristic values.

In the single crystal and feed rod:

$$-Pe_i\frac{\partial T_i}{\partial z}=\frac{1}{r}\frac{\partial}{\partial r}\left(\kappa_i r\frac{\partial T_i}{\partial r}\right)+\frac{\partial}{\partial z}\left(\kappa_i\frac{\partial T_i}{\partial z}\right)+\tfrac{1}{2}\alpha_i N_Q(A_i\cdot A_i^*) \quad i=\text{s, f} \tag{3}$$

In the melt:

$$\frac{1}{r}\frac{\partial}{\partial r}\left(\kappa_m r\frac{\partial T_m}{\partial r}\right)+\frac{\partial}{\partial z}\left(\kappa_m\frac{\partial T_m}{\partial z}\right)+\tfrac{1}{2}\alpha_m N_Q(A_m\cdot A_m^*)=0. \tag{4}$$

The last terms in the above equations are the heat generation rate by the Joulean heating, where A^* is the complex conjugate of A. N_Q is a non-dimensional number defined by

$$N_Q=\frac{\alpha_s'\omega^2\mu_0 J_c'^2 R_s^6}{\kappa_s' T'_{melt}} \tag{5}$$

where T'_{melt} is the melting point temperature of silicon. Pe is the Peclet number, and represents the non-dimensional crystal growth rate. It is defined by

$$Pe=\rho c_p V\frac{R_s}{\kappa_s'}. \tag{6}$$

V is the rate at which the melting zone moves downward.

The boundary conditions for temperature fields are expressed as follows.

At the melt–single-crystal and melt–feed-rod interfaces:

$$-\kappa_m\frac{\partial T_m}{\partial n}+\kappa_i\frac{\partial T_i}{\partial n}=\pm Pe_i St(\mathbf{e}_z\cdot\mathbf{n}) \tag{7}$$

$i=$ s or f

$$T_m=T_i=1. \tag{8}$$

At the melt free surface and crystal surface:

$$-\kappa_i\frac{\partial T_i}{\partial n}=Ra_i(T_i^4-T_a^4), \quad i=\text{m, s or f.} \tag{9}$$

At the ends of the feed-rod and the single crystal:

$$\frac{\partial T_i}{\partial n} = 0, \quad i = \text{s or f.} \tag{10}$$

In equation (7), the sign of the right-hand side is negative for the single crystal 's', and positive for the feed-rod '*f*'. The length of the feed-rod and the single crystal should be long enough that the boundary condition, equation (10), is satisfied. *St* is the Stefan number and *Ra* is the radiation number. *St* is given by

$$St = \frac{\Delta H_f}{c_p T'_{melt}} \tag{11}$$

and *Ra* is revealed by

$$Ra_i = \frac{\alpha'_i \varepsilon_1 T'_{melt} R_s}{\kappa'_s}, \quad i = \text{m, s or f.} \tag{12}$$

All interface coordinates in the system are also treated as part of the solution. The coordinates of the melt–single crystal and melt–feed-rod interfaces are determined so that equation (8) is satisfied, i.e. the interfaces coincide with the melting isotherm. While the shape of the melt free surface can be determined by solving the equation for the normal force balance at the surface, i.e. the Young–Laplace equation taking the electromagnetic force into account;

$$2H = Bo\, z + \tfrac{1}{2} Bo_e B_s^2 + \lambda \tag{13}$$

where B_s is the non-dimensional tangential magnetic field at the surface. $2H$ is the mean curvature of the melt surface defined by the following equation with the radial distance, $r = f(z)$.

$$2H = \frac{f_{zz}}{(1+f_z^2)^{3/2}} - \frac{1}{f(1+f_z^2)^{1/2}}. \tag{14}$$

in which the subscript 'z' denotes the derivative d/dz. The two non-dimensional parameters, *Bo* and Bo_e, in equation (13) are defined by the following equations, and referred to as gravitational Bond number, and electromagnetic Bond number, respectively.

$$Bo = \frac{\rho_m g R_s^2}{\gamma}$$

$$Bo_e = \frac{\mu_0 J_c'^2 R_s^3}{\gamma}. \tag{15}$$

To solve equation (13), we assumed a constraint in which the growth angle φ_0 between the melt and single crystal is fixed to be a constant value, e.g. 11° in the case of silicon.

3. NUMERICAL METHODS

As the boundary in the electromagnetic phenomena should be placed at infinite distance, the finite element method (FEM), coupled with the boundary element method (BEM) which is suitable to deal with such a boundary, is used in the analysis of the electromagnetic field [7], while the standard Galerkin FEM is applied to the heat transfer analysis. In the following sections, we highlight the essential features of these methods.

3.1. *Formulation of FEM coupled with BEM for the electromagnetic field*

We first draw a mathematical boundary S to enclose the system as shown by the dashed lines in Fig. 2(a), and employ the finite element method in the interior region, 'V', of the boundary and the boundary element method in the exterior region.

The angular component of vector potential, A, in the interior region is approximated with the Lagrangian bilinear polynomials, ϕ_l, defined over a mesh consisting of four-node quadrilateral elements and nodal values, A_l, as follows,

$$A(r,z) = \sum_l \phi_l A_l. \tag{16}$$

Application of the Galerkin weighted residual method and equation (16) to equation (1) yields a set of algebraic equations as follows.

$$\int_{r_i} \frac{\partial \phi_k}{\partial r}\frac{\partial A_i}{\partial r} r\,dr\,dz + \int_{r_i} \frac{\partial \phi_k}{\partial z}\frac{\partial A_i}{\partial z} r\,dr\,dz + \int_{r_i} \phi_k \frac{A_i}{r^2} r\,dr\,dz + jN_A \int_{r_i} \phi_k \alpha_i A_i r\,dr\,dz - \int_{r_i(i=c)} \phi_k r\,dr\,dz - \int_s \phi_k q r\,dS = 0$$

$$i = \text{s, m, f, c or a} \tag{17}$$

where q is the normal derivative of A at the boundary S. The integrals in equation (17) are evaluated numerically by nine-point Gaussian quadrature.

In the exterior region of the boundary S, the boundary element method is employed. First, we introduce the response function G satisfying the following equation.

$$\nabla^2 G - \frac{G}{r^2} = -\delta(r-r_0, z-z_0) \tag{18}$$

where G corresponds to the angular component of the vector potential at (r,z) excited by a circular line current located at (r_0, z_0) in free space, and represented by the complete elliptic integrals of the first and second kinds, $K(k)$ and $E(k)$, and $k^2 = 4rr_0/[(r+r_0)^2 + (z-z_0)^2]$, as follows:

$$G = \frac{1}{\pi k}\sqrt{\frac{r_0}{r}}\left\{\left(1-\frac{k^2}{2}\right)K(k) - E(k)\right\}. \tag{19}$$

Multiplying equation (1) with subscript 'a' by G and equation (18) by A, subtracting the resulting equations, and integrating them over the exterior region with Green's theorem, a line integral equation defined on the r–z plane is obtained. Then, the line integral equation is applied to the point (r_0, z_0) just on the boundaries which are shown by the dashed lines

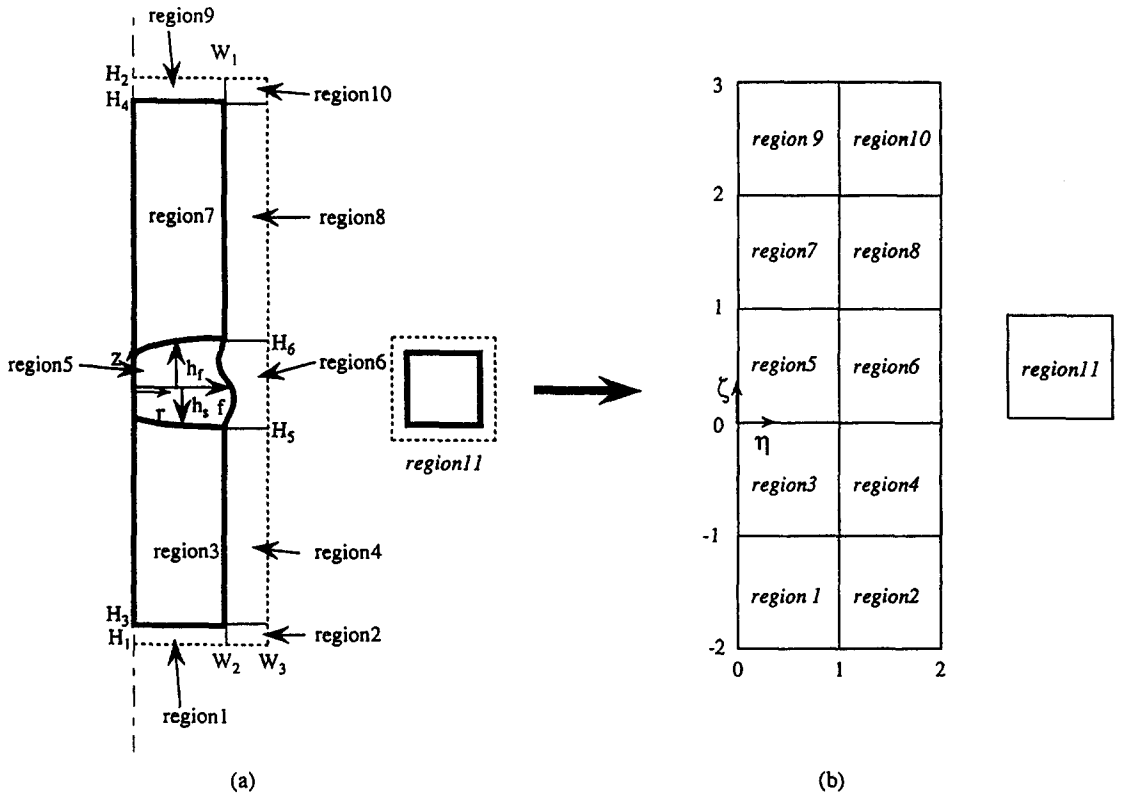

Fig. 2. Schematic diagram of coordinate transformation.

in Fig. 2(a). After a little algebra to overcome the singularity, the following integral equation is obtained [7]:

$$\int_s \left(G\frac{\partial A}{\partial n} - A\frac{\partial G}{\partial n} \right) r \, \mathrm{d}s = \tfrac{1}{2} r_0 A(r_0, z_0). \tag{20}$$

To discretize equation (20), we divide the boundaries into one-dimensional elements by the nodal points used in the FEM and set sampling points at the center of each element. When we assume that A and $\partial A/\partial n$ are uniform across each section, then equation (20) is modified as follows.

$$[F]\{q\} - [H]\{A\} = \{0\}. \tag{21}$$

The elements of the matrices $[F]$ and $[H]$ are given by

$$F_{ij} = \begin{cases} \displaystyle\int_s G r \, \mathrm{d}s = G_{ij} r_j w_j & i \neq j \\ \displaystyle\frac{w_i}{2\pi}\left(\ln \frac{16 r_i}{w_i} - 1 \right) & i = j \end{cases} \tag{22}$$

$$H_{ij} = \begin{cases} \displaystyle\int_s \frac{\partial G}{\partial n} r \, \mathrm{d}s = \left(\frac{\partial G}{\partial n} \right)_{ij} r_j w_j & i \neq j \\ \tfrac{1}{2} r_i & i = j \end{cases} \tag{23}$$

where r_i denotes the r coordinate of the ith sampling point and w_i is the length of the ith section. For the coupling of the BEM with the FEM, the following should be satisfied, that the normal derivatives, q, across each element on the boundary between the interior and exterior regions are continuous.

3.2. *Formulation of FEM in heat transfer analysis*

Temperature fields in the melt, single crystal and feed rod are approximated by Lagrangian bilinear polynomials, ϕ_1, where the same meshes as the four-node quadrilateral elements in the electromagnetic field are used.

$$T(r, z) = \sum_1 \phi_1 T_1. \tag{24}$$

The Galerkin weighted residual method and the solution approximation, equation (24), yield a set of algebraic equations given by

$$-Pe_i \int_{v_i (i \neq \mathrm{m})} \phi_\mathrm{k} \frac{\partial T_i}{\partial z} r \, \mathrm{d}r \, \mathrm{d}z + \int_{v_i} \kappa_i \frac{\partial \phi_k}{\partial r} \frac{\partial T_i}{\partial r} r \, \mathrm{d}r \, \mathrm{d}z + \int_{v_i} \kappa_i \frac{\partial \phi_\mathrm{k}}{\partial z} \frac{\partial T_i}{\partial z} r \, \mathrm{d}r \, \mathrm{d}z - \frac{N_\mathrm{Q}}{2} \int_{v_i} \phi_\mathrm{k} \alpha_i (A_i \cdot A_i^*) r \, \mathrm{d}r \, \mathrm{d}z - \int_{s_{\mathrm{B}i}} \kappa_i \phi_\mathrm{k} \frac{\partial T_i}{\partial z} r \, \mathrm{d}S = 0 \quad i = \mathrm{s, m \text{ or } f} \tag{25}$$

where $S_{\mathrm{B}i}$ represents the boundary surface of V_i. In the present analysis, the mesh is defined so that interfacial boundaries always lie along element edges; indeed, the mesh location itself is a part of the solution. The

melt surface shapes and the melt–feed-rod and melt–single crystal interface shapes are approximated using the one-dimensional Lagrangian linear function Γ_l, which are defined along the appropriate edges of the two-dimensional quadrilateral elements,

$$f = \sum_l \Gamma_l f_l \tag{26}$$

$$h_i = \sum_l \Gamma_l h_{il} \quad i = \text{s or f.} \tag{27}$$

The residual equations to determine the shapes of the interfaces and melt free surface are given as follows:

$$\int \Gamma_k (T-1) r \, dS = 0 \quad i = \text{s or f} \tag{28}$$

$$\int [\Gamma_k \{2Hf(1+f_z^{1/2})+1\} + (\Gamma_k f_z + f\Gamma_{kz}) \tan^{-1} f_z] \, dz = 0. \tag{29}$$

3.3. *Coordinate transformation method*

As the interface shapes are part of the solution, the electromagnetic and temperature fields are implicitly affected by the shapes. We make the dependencies of the equations on the interface shapes explicit by transforming the equation set to the fixed cylindrical region in the (η, ζ) coordinate system [1]. As shown in Fig. 2(b), the calculation region is divided into eleven regions. The coordinates of region 11 including the RF coil are not transformed because this region is isolated from other regions and is unaffected by the deformation of the interfaces. Ten other regions are needed to transform the coordinate so that the boundaries of each region always lie along the boundary surfaces in the system. The coordinate transformation from the physical domain (r, z) to the transformed domain (η, ζ) was carried out with the aglebraic expressions which relate (r, z) to (η, ζ) as listed in Table 1.

Table 1. Coordinate transformations in ten regions

	$r \to \eta$	$z \to \zeta$
region 1	$\eta = r/W_2$	$\zeta = ,(z-H_1)/(H_3-H_f)-2$
region 2	$\eta = (r-W_2)/(W_3-W_2)+1$	$\zeta = (z-H_1)/(H_3-H_1)-2$
region 3	$\eta = r/W_2$	$\zeta = (z-H_3)/(h_s-H_3)-1$
region 4	$\eta = (r-W_2)/(W_3-W_2)+1$	$\zeta = (z-H_3)/(H_5-H_3)-1$
region 5	$\eta = r/f$	$\zeta = (z-h_s)/(h_f-h_s)$
region 6	$\eta = (r-f)/(W_3-f)$	$\zeta = (z-H_5)/(H_6-H_5)$
region 7	$\eta = r/W_1$	$\zeta = (z-h_f)/(H_4-h_f)+1$
region 8	$\eta = (r-W_1)/(W_3-W_1)+1$	$\zeta = (z-H_6)/(H_4-H_6)+1$
region 9	$\eta = r/W_2$	$\zeta = (z-H_4)/(H_2-H_4)+2$
region 10	$\eta = (r-W_1)/(W_3-W_1)+1$	$\zeta = (z-H_4)/(H_2-H_4)+2$

3.4. *Iterative solution*

The complete set of the discretized equations with the coordinate transformation described in the previous section is represented as follows.

$$\mathbf{R}(\mathbf{x}; \mathbf{p}) = 0 \tag{30}$$

where $\mathbf{R}$ is the vector of residual equations whose Jacobian has the 'arrow' matrix with a banded structure augmented with several full columns and raws, $\mathbf{x}$ is the vector of the unknowns, i.e. vector potential, temperature and all interface shapes, $\mathbf{p}$ represents the model parameters, such as crystal growth rate, dimensionless heat generation rate and so on. Since the residual equations are nonlinear due to radiation heat transfer and the free boundaries, an iterative method, i.e. Newton's procedure, must be employed for solution.

4. NUMERICAL RESULTS

In the present work, the analyses of heat transfer in silicon FZ growth system with a RF heating as shown in Fig. 1 were carried out, with the diameter of both feed-rod and single crystal both set to 1 cm. Physical properties of silicon are listed in Table 2.

First, we demonstrate that the coordinate transformation method described in Section 3 is useful for the heat transfer analysis of the RF FZ growth system. Figure 3(a) shows the temperature distributions and the shape of molten zone, where the RF coil current density, J_c', is 1.93×10^7 A m^{-2} and the growth rate, V, is 4.57×10^{-5} m s^{-1} and the frequency of the RF coil, ω, is 1.3 MHz, and no electromagnetic force acts on the melt surface ($Bo_e = 0$). The finite element meshes in this system are shown in Fig. 3(b). The meshes, except for the RF coil domain, deform so that they coincide with the phase boundaries. The shape of the melt surface is remarkably deformed. The melt

Table 2. Physical properties of silicon

Melting point	T_{melt}'	1683 [K]
Latent heat solidification of solidification	ΔH_f	1.8×10^6 [J kg^{-1}]
Thermal conductivity of melt	κ_m'	64 [W m^{-1} K^{-1}]
Thermal conductivity of feed	κ_f'	21.8 [W^{-1} mK^{-1}]
Thermal conductivity of single crystal	κ_s'	21.8 [W m^{-1} K^{-1}]
Electrical conductivity of melt	α_m'	1.0×10^6 [S m^{-1}]
Electrical conductivity of feed	α_f'	1.2×10^6 [S m^{-1}]
Electrical conductivity of single crystal	α_s'	1.2×10^6 [S m^{-1}]
Magnetic permeability	μ_0	1.257×10^{-6} [H m^{-1}]
Density of melt	ρ_m	2420 [kg m^{-3}]
Density of feed and single crystal	$\rho_{f\text{ and }s}$	2300 [kg m^{-3}]
Surface tension	γ	7.2×10^{-1} [N m^{-1}]
Contact angle	φ_0	11 [deg]

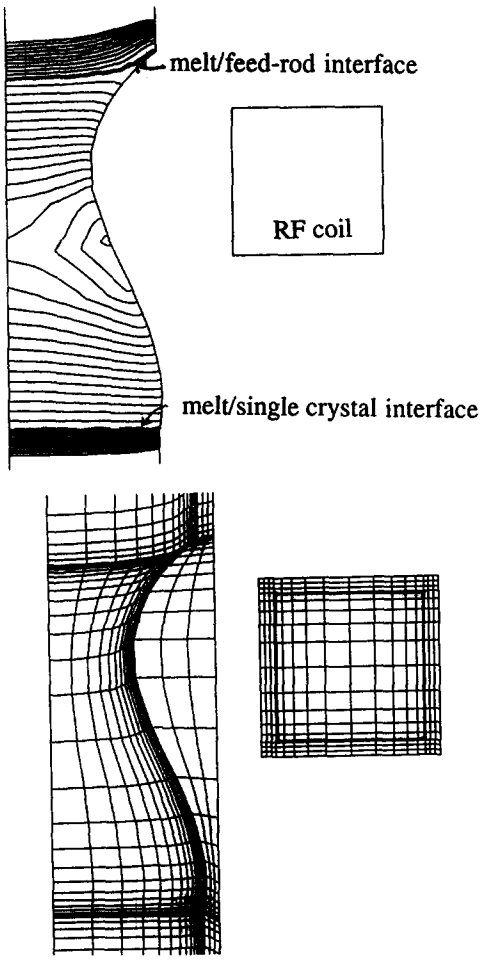

Fig. 3. (a) Temperature field in the molten zone and the interface shapes for $J'_c = 1.93 \times 10^7$ A m^{-2} and $Bo_e = 0$. (b) Finite element discretization.

zone in the figure corresponds to the longest one up to which the molten zone is stable under the above-mentioned processing parameters.

Figure 4 shows the effect of the current density in the RF coil, J'_c, on the temperature fields and the shapes of molten zone, where the frequency of the RF

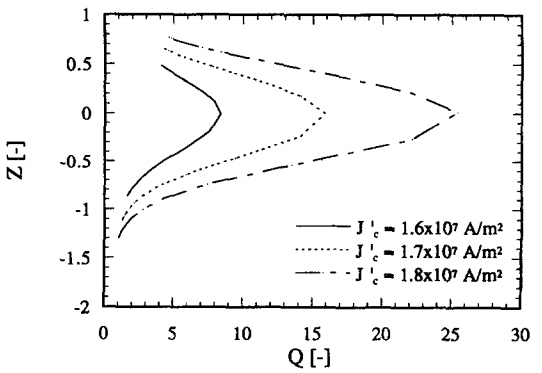

Fig. 5. Effect of J'_c on heat generation rate along the surface by Joulean heating for $\omega = 1.3$ MHz and $V = 4.57 \times 10^{-5}$ m s^{-1}.

current in the coil, ω, is 1.3 MHz, the growth rate, V, is 4.57×10^{-5} m s^{-1} and the electromagnetic force induced by the RF current acts on the melt surface. As the electromagnetic Bond number, Bo_e, is proportional to J'^2_c as shown in equation (15), Bo_e becomes large with J'_c. The melt length increases as J'_c increases since the heat generation rate along the surface by Joulean heating increases as shown in Fig. 5. The RF coil is placed between $Z = -0.5$ and 0.5 in Fig. 5. The heating power is the largest beside the center of the coil, but from Fig. 4, the point with the maximum temperature in the melt and thus the center of the molten zone is slightly below the center of the coil, because of the effect of the latent heat of fusion and solidification at each phase boundary.

As was mentioned earlier, the electromagnetic field generated by the RF current plays an important role in the determining shape and stability of the molten zone through the electromagnetic force, which is generally considered to stabilize the melt because it is directed inward. To investigate the effect of the electromagnetic force in the RF FZ system, we calculate the case of $Bo_e = 0$ and compare it with the results in Fig. 4. Figure 6 shows the temperature distributions and the shapes of the molten zone calculated with the same processing parameters as in Fig.

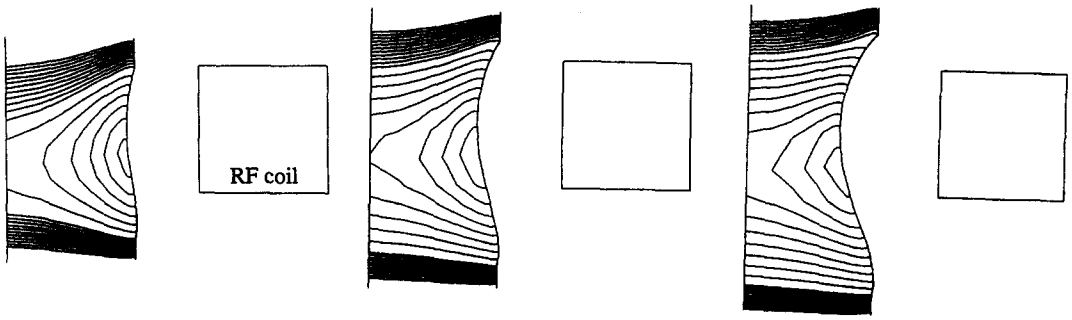

J'$_c$=1.6x10^7 A/m^2 (Bo$_e$=55.9)

J'$_c$=1.7x10^7 A/m^2 (Bo$_e$=63.1)

J'$_c$=1.8x10^7 A/m^2 (Bo$_e$=70.7)

Fig. 4. Effect of the RF current density on the temperature fields and the shape of molten zone ($\Delta T = 0.002$).

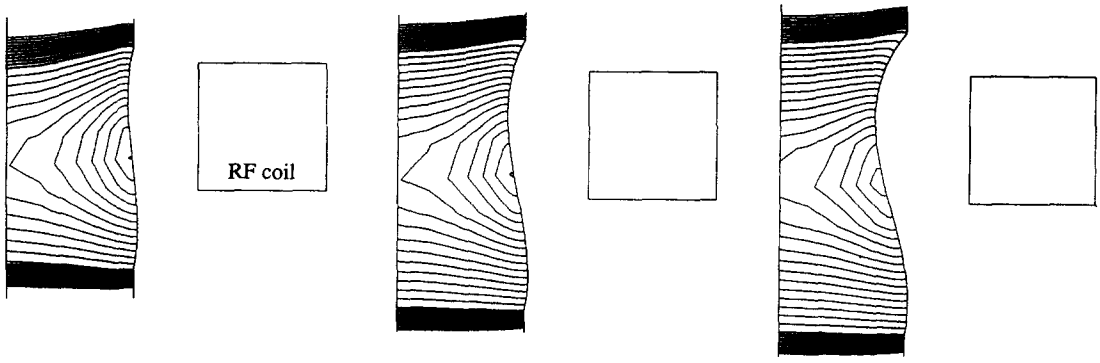

Fig. 6. Effect of J_c' on the temperature fields and the shape of molten zone for $Bo_e = 0$ ($\Delta T = 0.002$).

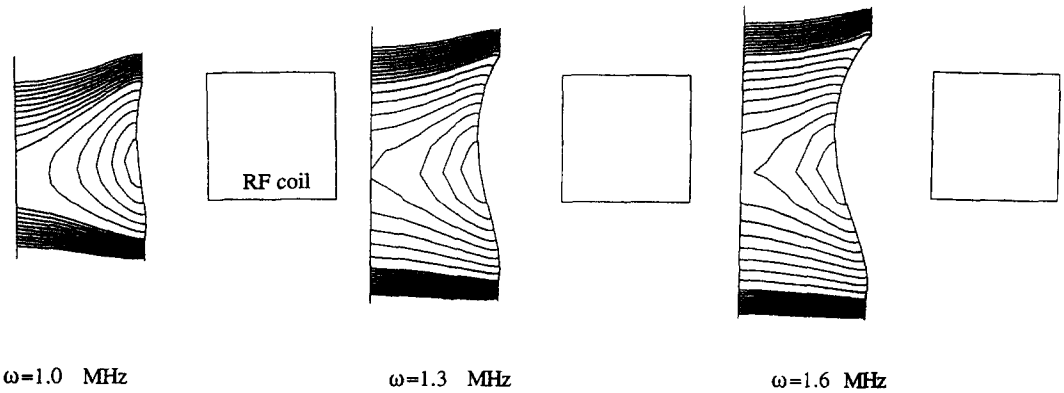

Fig. 7. Effect of the current frequency in the RF coil on the temperature fields and the shape of molten zone ($\Delta T = 0.002$).

4 except for $Bo_e = 0$. The length of molten zone is longer and the average temperature in the melt is higher in comparison with the results in Fig. 4. Also, we notice that the melt surface with non-zero Bo_e is more remarkably deformed inward due to the electromagnetic force acting on the melt surface, compared with the results for $J_c' = 1.8 \times 10^7$ in Fig. 4 and for 1.7×10^7 A m^{-2} in Fig. 6 which have almost the same melt lengths.

Figure 7 shows the effect of the applied RF frequency on the temperature field and the shapes of molten zone for $J_c' = 1.7 \times 10^7$ A m^{-2} and $V = 4.57 \times 10^{-5}$ m s^{-1}. This figure reveals that the melt length becomes longer as the frequency increases. The distributions of the heat generation rate along the surface are also shown in Fig. 8.

In the FZ crystal growth process, the stability of the molten zone is very important for the operation. Figure 9 shows the calculated diagram for the upper and lower limits of the RF current density in the coil between which the molten zone can be formed stably. Below the lower limit of J_c' for a given ω, the zone is not completely melted and a solid core remains in the center. While beyond the upper limit, the molten zone becomes unstable and will separate into two hemispheres attached to the rods. From Fig. 9, both the upper and lower limits of J_c' decrease as ω increases.

Figure 10 shows the effect of the rate of crystal growth on the temperature distributions in the melt and the shapes of the molten zone, where J_c' is 1.7×10^7 A m^{-2} and ω is 1.3 MHz. The length of the molten zone is not so sensitive to the rate of crystal growth. On the other hand, the feed-melt interface becomes

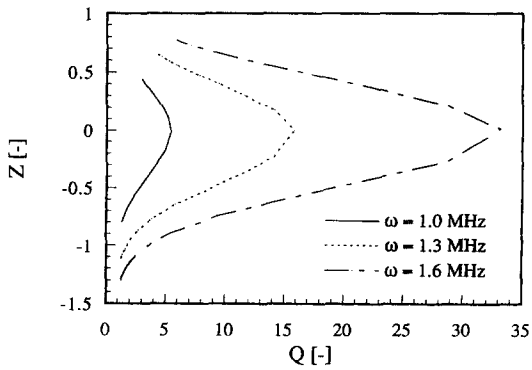

Fig. 8. Effect of ω on heat generation rate along the surface by Joulean heating for $J_c' = 1.7 \times 10^7$ A m^{-2} and $V = 4.57 \times 10^{-5}$ m s^{-1}.

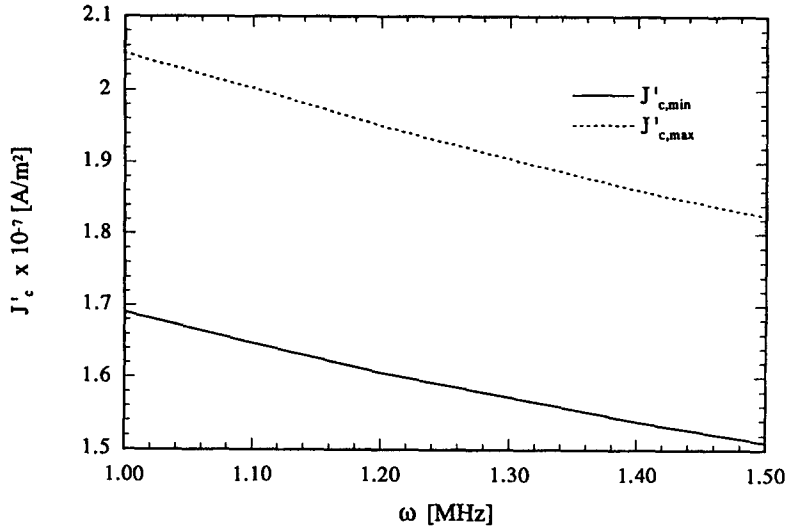

Fig. 9. Diagram for the upper and lower limits of J_c' in an RF FZ system.

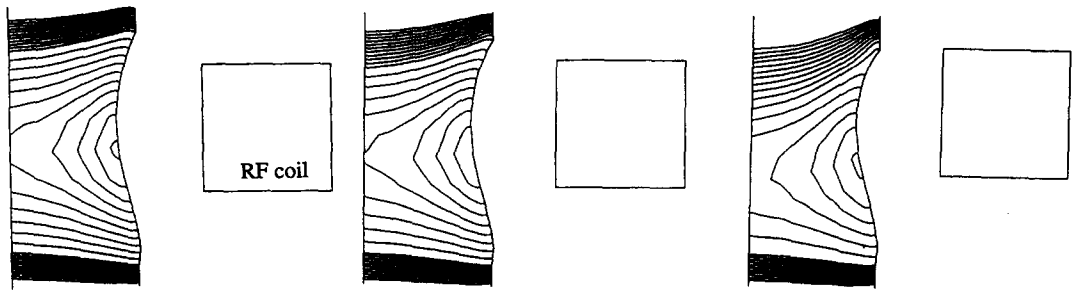

$V=2.29\times10^{-5}$ m/s $V=4.57\times10^{-5}$ m/s $V=9.14\times10^{-5}$ m/s

Fig. 10. Effect of crystal growth rate on the temperature fields and the shape of molten zone for $J_c' = 1.7\times10^7$ A m^{-2} and $\omega = 1.3$ MHz ($\Delta T = 0.002$).

more convex to the melt, and the molten zone moves down relative to the RF coil due to the effect of the latent heat at the interfaces.

5. CONCLUSIONS

We have developed a method for calculating the radio frequency floating zone processes. Finite element method and boundary element method are combined to calculate the electromagnetic and temperature fields. A coordinate transformation is useful to analyze a RF FZ system with deformed interface shapes. The effects of the current density and frequency of RF coil and of the rate of crystal growth on the temperature field and interface shapes in the FZ system were investigated numerically. From the numerical results, the electromagnetic forces acting on the melt surface affect the shapes of the molten zone. We also obtained a diagram for the upper and lower limits of the forced current density in the RF coil between which the molten zone can be stable.

Acknowledgements—This study is carried out as a part of "Space Utilization Frontiers Joint Research Projects" promoted NASDA.

REFERENCES

1. J. L. Duranceau and R. A. Brown, Thermal-capillary analysis of small-scale floating zones: steady-state calculations, *J. Crystal Growth* **75,** 367–389 (1986).
2. C. W. Lan and S. Kou, Heat transfer, fluid flow and interface shapes in floating-zone crystal growth, *J. Crystal Growth* **108,** 351–366 (1991).
3. C. W. Lan and S. Kou, Effect of rotation on radial dopant segregation in microgravity floating-zone crystal growth, *J. Crystal Growth* **133,** 309–321 (1993).
4. C. W. Lan and S. Kou, Radial dopant segregation in zero-gravity floating-zone crystal growth, *J. Crystal Growth* **132,** 578–591 (1993).
5. A. Mühlbauer, W. Erdman and W. Keller, Electrodynamics in silicon floating zones, *J. Crystal Growth* **64,** 529–545 (1983).
6. D. N. Riahi and J. S. Walker, Float zone shape and stability with the electromagnetic body force due to a radio-frequency induction coil, *J. Crystal Growth* **94,** 635–642 (1989).
7. T. Miyoshi, M. Sumiya and H. Omori, Analysis of an induction heating system by the finite element method combined with a boundary integral equation, *IEEE Trans. Magnetics*, **MAG-23,** 1827–1832 (1987).